International Forum on Aeroelasticity and Structural Dynamics
IFASD 2019
9-13 June 2019, Savannah, Georgia, USA

HIGH BANDWIDTH MORPHING ACTUATOR FOR EXPERIMENTAL AEROELASTIC CONTROL

Irma Isnardi[1] **and Sebastiano Fichera**[1]

[1]School of Engineering, University of Liverpool,
Liverpool, L69 3GH, UK
irma.isnardi@liverpool.ac.uk
s.fichera@liverpool.ac.uk

Keywords: morphing, active aeroelastic control, receptance method, flutter suppression, piezoceramic patches.

Abstract: This paper presents the installation and wind tunnel testing of a camber-morphing trailing edge system on an aeroelastic wing. Such morphing system, called High Bandwidth Morphing Actuator (HBMA), is capable of achieving actuation frequencies up to 25 Hz with varying amplitudes. The installation of the morphing actuator in the aeroelastic rig is firstly achieved. Then the aeroelastic behaviour of the entire system is assessed and an active controller is designed, by using the Receptance Method, with the aim of increasing the damping of the first bending and torsional modes. The HBMA proved to be capable of introducing the desired control input that resulted in an increase the flutter velocity up to 10%.

1 INTRODUCTION

Numerous solutions have been explored over the past years for achieving continuous aerofoil camber deformation, the initial feasibility studies on aerofoil morphing with piezoelectric materials were carried out by Lazarus et al. [1], who altered a typical wing box section utilising strain-actuated adaptive structures. During the early 2000s, new morphing actuators with continuous flaps and skin-embedded piezo-patches were produced as result of the development by the NASA Langley Research Centre of the Macro-Fiber Composite (MFC) [2, 3] and the rising interest in camber-morphing aerofoil. Amongst them, Bilgen et al. developed a bidirectional variable-camber aerofoil employing eight MFC 8557-P1 patches in a bimorph configuration to construct the active surfaces, and a single four-bar (box) mechanism for skin compliance [4]. Molinari et al. [5] designed and tested a lightweight wing where three piezoceramic patches control the roll by deforming the aerofoil camber. Debiasi et al. aimed to morph the entire camber of the aerofoil applying four MFC 8557-P1 patches in pairs to the upper and lower surface. The section studied was a NACA 0015 with skin compliance achieved by linear sliders inside the leading edge of the aerofoil [6]. More recently, the modification of the aerofoil section is used to optimise the aerodynamics at the different flight phases or to improve the aircraft controllability [7]. However, most of the solutions proposed show scalability issues and are not designed for controlling responses in the frequency range of interest for gust loads alleviation and flutter suppression. To address the latter problem, the authors recently proposed a High Bandwidth Morphing Actuator (HBMA) capable of achieving actuation frequencies up to 25 Hz with varying amplitudes [8].

This work builds upon such morphing design and presents its tailoring and installation on an aeroelastic test rig developed at the University of Liverpool called MODFLEX (MODular aeroe-

lastic FLEXible wing) [9]. Wind tunnel test are then conducted for demonstrating the effectiveness of the proposed actuator for active aeroelastic control.

The paper is organised as follow: after this introduction, in Section 2 the MODFLEX aeroelastic system is briefly introduced, together with the description of the HBMA system and its installation within the wind tunnel rig. Section 3 summarises the controller technique adopted and Section 4 presents the experimental wind tunnel tests together with the results achieved in terms of flutter suppression.

2 AEROELASTIC SYSTEM

The morphing aerofoil actuator capable of aeroelastic control is experimentally tested on an aeroelastic flexible modular wing called MODFLEX. The aeroelastic model was designed as a typical flexible and finite-length wing and it presents a classical flexural-torsional flutter at low airflow velocity. The analytical aeroelastic model is described by the following equation:

$$\mathbf{M}\ddot{\mathbf{q}} + \mathbf{C}\dot{\mathbf{q}} + \mathbf{K}\mathbf{q} = q\mathbf{f_A} + \mathbf{B}\mathbf{u} \tag{1}$$

where $\mathbf{M}$, $\mathbf{C}$ and $\mathbf{K}$ are respectively the mass, damping and stiffness matrices, $\mathbf{f_A}$ is the vector of generalised aerodynamic forces (GAFs), $\mathbf{u}$ is the vector of control input and $\mathbf{B}$ is a matrix defining the control force distribution in the structure.

2.1 MODular aeroelastic FLEXible wing

The MODFLEX is made by a single aluminium-alloy spar that constitutes the only structural element of the model. The cross shape was chosen in order to obtain the desired flexural, torsional and in-plane stiffness so that the flutter velocity of the model is in the range 0-20 m/s. The main spar is covered by four sectors, with a NACA 0018 aerofoil, that provides the correct aerodynamic shape. The sectors have a chord of 0.3 m and the overall wingspan is 1 m. To keep unchanged the stiffness of the model, the sectors are linked to the main spar by two pins at the mid-span and they are assembled assuring a 2 mm gap between each others. The mass and flexural axes were designed to overlap on the main spar, at the mid-chord. The sectors are 3D-printed and made by ABS. A detailed description of the rig can be found in Ref [9] and the main model specifications are summarised in Table 1.

Table 1: MODFLEX main specifications.

Wing Data	Dimension
Wing span	1 m
Chord (c)	0.3 m
Aerofoil	NACA0018
Mass axis position	0.5c
Flexural axis position	0.5c

2.2 High Bandwidth Morphing Actuator design and configuration

The HBMA is composed by two parts, the upper portion are the MFC piezo-patches in a sandwich configuration and the lower is a 0.3 mm thickness stainless steel sheet. The MFC piezo-patch sandwich is formed by two glued MFCs, one for each side of a stainless steel sheet 0.012 mm thickness, the passive material is necessary to produce a bending behaviour, since the piezo material generates an in-plane effect. The two piezo-patches are bonded in an antagonistic layout to create symmetric deflection of the actuator, once operated around zero deflection. Such

configuration increases also the bending blocking force and the structural stiffness of the skin. The sandwich configuration has the disadvantage to decrease the maximum theoretical deflection generated by a single patch attached to the passive material due to the opposite behaviour of the two piezo-patches. The sheets are fixed at the main structure by L-shape ABS plastic brackets and at the other ends, a linear slider provides the accordance between the MFC and the stainless steel sheet. The slider was designed to allow $\pm$7.5 mm of linear sliding which ensures $\pm$20 degree or 20 mm of trailing edge displacement. The total dimensions of the actuator are 128 mm length (88 mm unsupported), 68 mm width, when using MFC M-8528-P1, and the total mass is 30 g. The actuation of MFC patches is achieved by applying an asymmetrical voltage between -500 V and +1500 V leading to symmetrical actuation behaviour. The maximum deflection is reached by supplying one MFC with +1500 V while the other with -500 V and vice versa for the opposite maximum deflection.

The HBMA is also capable of closed loop (CL) control of the morphed shape. A strain gauge is glued to the stainless steel sheet (opposite to the MFC-sandwich) and provides, after calibration, the feedback signal for the PID controller. Such control system is called Low Level Controller (LLC) and acts as an intermediate layer between the aeroelastic controller and the experimental model.

The HBMA design, development and tests are detailed in Ref [8]. Figure 1 shows a drawing of the actuator and its main components. The installation of the HBMA into MODFLEX rig

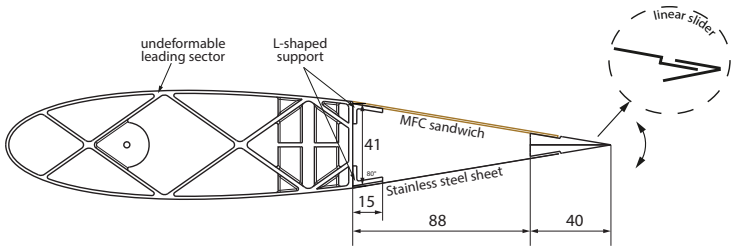

Figure 1: Side view of the actuator (dimensions in mm).

required some modification to the original design. Firstly, wider piezo patches, namely MFC M-8557-P1, have been used. To increase further the morphing span, two HBMAs are installed in the aeroealstic model. The two actuators are set in a mirrored configuration respect the mid-line to guarantee a symmetric behaviour of the overall system and a better control of the wing. Such configuration, with the two actuators positioned on the opposite sides of the aerofoil, made necessary to supply the voltage in an inverted way to guarantee a coherent movement of the control. In fact, the maximum up deflection of the upper actuator corresponds to the maximum down deflection of the lower one.

Figure 2 shows the HBMA configuration in the experimental setup, the fourth sector is equipped with the camber-morphing trailing edge system. The gaps between the two HBMAs are filled with six L-shaped stainless steel sheets of 0.3 mm thickness. The two actuators are placed symmetrically in the centre of the fourth sector, one actuator featuring the piezo element on the upper side and the other on the lower side of the aerofoil. The central stainless steel plate is connected to the left and right actuators to increase the overall span of the morphing system. The reduction of the maximum achievable tip deflection is compensated by the increase of the morphable span.

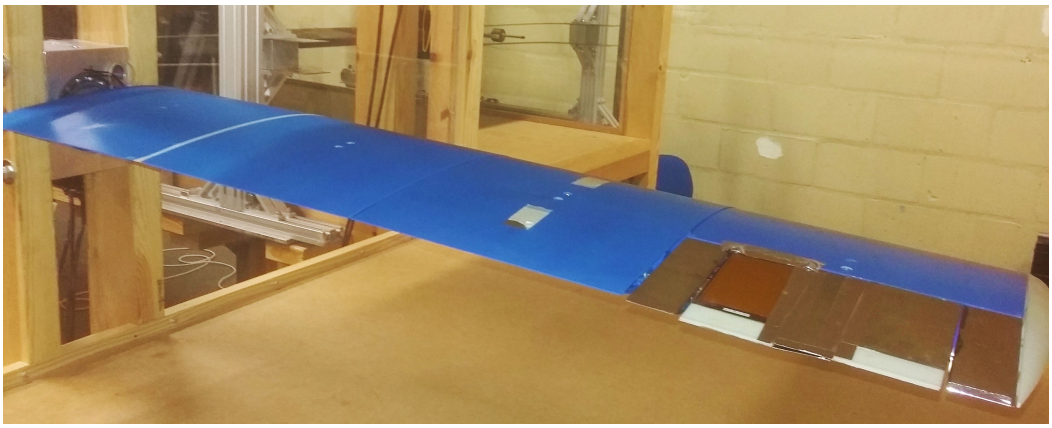

(a)

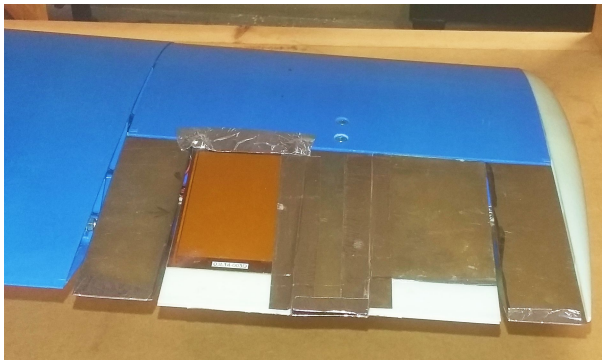

(b)

Figure 2: MODFLEX experimental setup.

3 POLE PLACEMENT WITH RECEPTANCE METHOD

To demonstrate that the morphing actuator is suitable for active aeroelastic control purposes, a feedback controller is implemented on the system described in Section 2 with the aim of rising the flutter speed by increasing the damping of the first bending and torsion modes. To design the gains for achieving such pole-placement, the Receptance Method is used.

The Receptance Method was introduced by Ram and Mottershead [10] and can be applied to any dynamic system once its receptances are known. To implement this active control technique is not necessary to know the system mass, damping, stiffness matrices ($\mathbf{M}$, $\mathbf{C}$, $\mathbf{K}$), or to have a state observer to evaluate unknown state variables, but only the experimental transfer functions are required. For an aeronautical systems, this means that no approximated form of the unsteady aerodynamic forces is required. The number of sensors determine the number of pole pairs that can be assigned.

Considering Eq. 1, and including in the system mass, damping, stiffness matrices the aerodynamic contribution ($\tilde{\mathbf{M}}$, $\tilde{\mathbf{C}}$, $\tilde{\mathbf{K}}$) and a control input with feedback gains $\mathbf{F}$, $\mathbf{G}$ as follow:

$$\mathbf{u} = \mathbf{F}^T\dot{\mathbf{q}} + \mathbf{G}^T\mathbf{q} \tag{2}$$

can be written as Eq. 1:

$$\tilde{\mathbf{M}}\ddot{\mathbf{q}} + \tilde{\mathbf{C}}\dot{\mathbf{q}} + \tilde{\mathbf{K}}\mathbf{q} = \mathbf{B}(\mathbf{F}^T\dot{\mathbf{q}} + \mathbf{G}^T\mathbf{q}) \tag{3}$$

If the matrices $\tilde{\mathbf{M}}$, $\tilde{\mathbf{C}}$, $\tilde{\mathbf{K}}$ are known, it is possible to choose arbitrarily the pole of the system and to tune the feedback gains $\mathbf{F}$, $\mathbf{G}$. However, in most cases, it is known only the transfer

function matrix between the control input forces and the displacement at a limited number of degrees of freedom. In this situation, the method defines a procedure to determine the feedback gains $\mathbf{F}$, $\mathbf{G}$ by using only the measured receptances.

The receptance method is a partial pole placement approach, where the first p poles are assigned (μ_k, $k = 1, \ldots, p$) and the open loop poles (λ_k, $k = p+1, \ldots, 2n$) remain unchanged; $\mathbf{r}(s) = \mathbf{H}(s)\mathbf{B}$ is the measured transfer-function matrix between the control input and output and $\mathbf{H}(s) = (\mathbf{M}s^2 + \mathbf{C}s + \mathbf{K})^{-1}$ is the receptance transfer-function matrix between the control inputs and outputs. For the Multi-Input-Multi-Output (MIMO) case, the control gains $\mathbf{F} = \begin{bmatrix}\mathbf{f_1} & \mathbf{f_1} & \ldots & \mathbf{f_m}\end{bmatrix}$, $\mathbf{G} = \begin{bmatrix}\mathbf{g_1} & \mathbf{g_1} & \ldots & \mathbf{g_m}\end{bmatrix}$ are given by solving the linear equation:

$$\begin{bmatrix} \mathbf{P_1} \\ \vdots \\ \mathbf{P_m} \\ \mathbf{Q_{p+1}} \\ \vdots \\ \mathbf{Q_{2n}} \end{bmatrix} \begin{pmatrix} \mathbf{f_1} \\ \vdots \\ \mathbf{f_m} \\ \mathbf{g_1} \\ \vdots \\ \mathbf{g_m} \end{pmatrix} = \begin{pmatrix} \alpha_1 \\ \vdots \\ \alpha_m \\ 0 \\ \vdots \\ 0 \end{pmatrix} \tag{4}$$

where

$$\mathbf{P_k} = \begin{bmatrix} \mu_k \mathbf{w_k}^T & 0 & \ldots & 0 & \mathbf{w_k}^T & 0 & \ldots & 0 \\ 0 & \mu_k \mathbf{w_k}^T & \ldots & 0 & 0 & \mathbf{w_k}^T & \ldots & 0 \\ \vdots & \vdots & \ddots & \vdots & \vdots & \vdots & \ddots & \vdots \\ 0 & 0 & \ldots & \mu_k \mathbf{w_k}^T & 0 & 0 & \ldots & \mathbf{w_k}^T \end{bmatrix} \tag{5}$$

$$\mathbf{Q_k} = \begin{bmatrix} \lambda_k \mathbf{v_k}^T & 0 & \ldots & 0 & \mathbf{v_k}^T & 0 & \ldots & 0 \\ 0 & \lambda_k \mathbf{v_k}^T & \ldots & 0 & 0 & \mathbf{v_k}^T & \ldots & 0 \\ \vdots & \vdots & \ddots & \vdots & \vdots & \vdots & \ddots & \vdots \\ 0 & 0 & \ldots & \lambda_k \mathbf{v_k}^T & 0 & 0 & \ldots & \mathbf{v_k}^T \end{bmatrix} \tag{6}$$

and

$$\mathbf{w_k} = \alpha_{\mu_k,1}\mathbf{r_{k,1}} + \alpha_{\mu_k,2}\mathbf{r_{k,2}} + \cdots + \alpha_{\mu_k,m}\mathbf{r_{k,m}} \qquad k = 1, 2, \ldots, p \tag{7}$$

the retained eigenvectors are denoted by $\mathbf{v_k}$. A careful choice of the weighting parameters ($\alpha_{\mu_k,j}$, $k = 1, \ldots, p$, $j = 1, \ldots, m$) determines the eigenvectors of the assigned model by Eq. 7 and it can minimise the control effort. As mentioned before, the method does not require to know $\mathbf{M}$, $\mathbf{C}$, $\mathbf{K}$ of the system, but it is necessary to evaluate only the frequency response function $\mathbf{H}(s)$ at the locations of the desired poles, $s = \mu_k$. For a Single Input case, m = 1 and α_{μ_k} can be chosen equal to 1. The method described here represents the High Level Controller (HLC) that is used as active aeroelastic controller in this work.

4 RESULTS

4.1 Experimental Setup

The experimental setup is schematically represented with the block diagram in Figure 3. On the left-side, as drawing of MODFLEX with the fourth sector equipped with the HBMA. Two laser displacement sensors mounted on the top of the wind tunnel measure the displacement of the wing in two points along the third sector (at 25% and 75% of the chord). The real time environment dSPACE is used for for A/D/A conversion and for implementing the Low and High Level Controllers. The laser displacement signals are filtered with a second-order Butterworth low-pass filter with a cut-off frequency of 15 Hz. The control signal to the morphing actuator is

amplified by two high voltage amplifiers AMT2012-CE3, one for each piezo-sandwich. Such amplifiers are able to rump up in the 0 / 5 V range to the necessary -500 / 1500 V up to a frequancy of 30 Hz. The reading form the strain gauge is fed back into the PID controller, implemented as well in dSPACE.

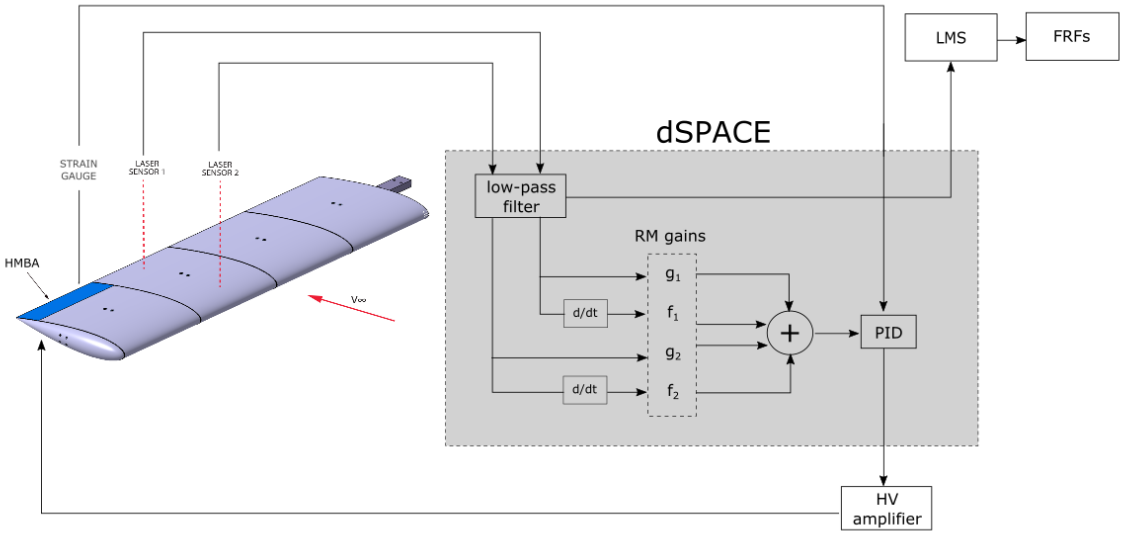

Figure 3: Experimental setup block scheme.

Before applying the High Level Controller to the system, the ability of the HBMA to follow a prescribed motion was investigated without applying the PID controller. The HBMA was supplied with a 1 Hz sinusoidal input at maximum deflection voltages and the displacement of the aerofoil tip recorded with a laser displacement sensor, together with the strain gauge readings. Figures 4(a) and 4(b) show the prescribed deflection against the measured tip displacement and the strain gauge readings against the measured tip displacement, respectively. The actuator is able to track the prescribed motion and the hysteresis, typical of the piezoelectric materials, seems not to affect significantly the general behaviour of the HBMA. Having assessed this, and due to some persistent issues with the PID tuning, the hereinafter test campaign was performed switching off the LLC.

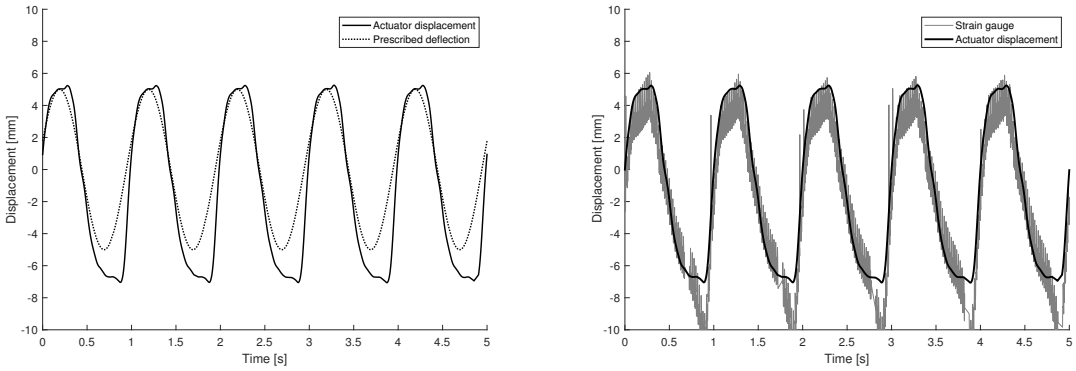

(a) Actuator displacement vs prescribed deflection. (b) Strain gauge reading vs. actuator displacement.

Figure 4: HBMA ability to follow a motion at 1 Hz.

4.2 V-g diagrams and Flutter test

The velocity vs. frequency (V-f) and velocity vs. damping (V-g) diagrams are obtained by computing frequency and damping of the first bending and torsional modes at different airspeeds. The aeroelastic model is tested at different airspeed from 0 to 12 m/s (close to the flutter speed) and open loop input-output FRFs are generated via a stepped-sine excitation introduced by the HBMA. The frequency range of interest is between 2 Hz and 6 Hz; the input is the voltage supplied to the piezo-patches and the outputs are the laser displacement sensor measurements. Such displacement signals are acquired by dSPACE and low-pass filtered before being provided to modal analysis systems (Siemens.PLM LMS equipped with Test.Lab) to compute the FRFs. The values of frequencies and damping are estimated by the modal parameter estimation technique PolyMAX [11]. Figure 5(a) and Figure 5(b) show, respectively, the V-f and V-g diagrams. By analysing the trend of the damping of the first torsional mode it is possible to see that it is approaching the zero value while the airspeed is increasing. In the 10-12 m/s airspeed range, the damping of the bending mode is behaving in an unexpected manner (decreasing instead of continuously increasing), this can be explained by the coalescence of the two modes approaching the flutter velocity that alters PolyMAX prediction.

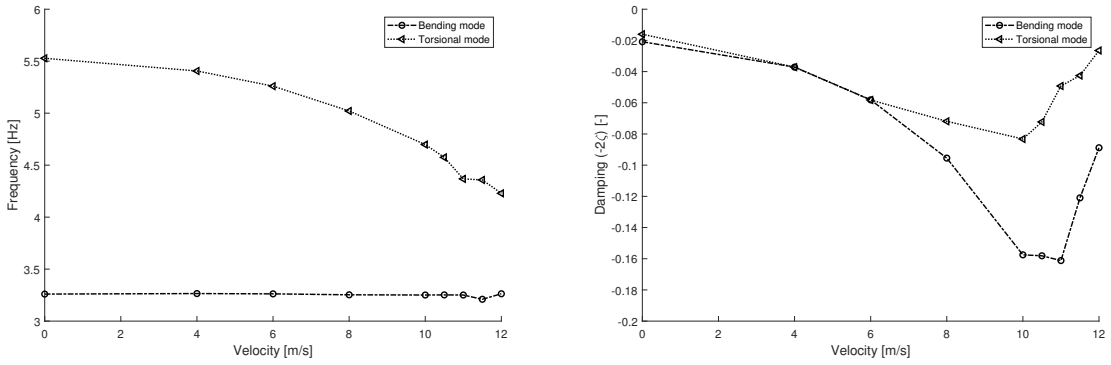

(a) Velocity vs. frequency diagram.

(b) Velocity vs. damping diagram.

Figure 5: V-f and V-g diagrams of the MODFLEX wing in Open Loop.

The experimental flutter velocity was evaluated as follow: the model was set with an initial airspeed of 12 m/s and then the airflow velocity was increased with 0.1 m/s increments until the model became unstable. The flutter velocity for the MODFLEX in the described configuration is 13.3 m/s.

4.3 Closed-loop tests

In this section the high level aeroelastic controller, designed following the method presented in Section 3 is applied to the experimental rig. As already mentioned, the systen is Single-Input-Multiple-Output (SIMO), where the input is the voltage supplied to the HBMA and the outputs are the laser readings, in voltage. To implement the receptance method, the input-output FRFs in open loop are necessary. Such FRFs are readily available because underpinning the V-g/V-f diagrams presented earlier. The controller is designed by using the input-output FRFs at 10 m/s - reasonably close to the flutter velocity, but not too close to have strong coalescence of the modes of interest. The FRFs are then fitted with stable minimum-phase transfer function, using SDTools toolbox, to determine the transfer function matrix of the system $\mathbf{r}(s)$. The control is designed for assigning (increasing) the damping of the first bending and torsional modes. The various control configuration implemented on the system and tested are summerised in Table

2, that also presents the comparison between the open loop and closed loop frequency and damping for the different tests carried out.

Table 2: First bending and torsional modes open loop vs. closed loop at airspeed 10 m/s. The error between the expected and registered values of frequency and damping for each test are in brackets.

	Tests	1^{st} bending mode		1^{st} torsional mode	
		Frequency [Hz]	Damping [%]	Frequency [Hz]	Damping [%]
	Open Loop	3.25	7.33	4.70	4.16
1	ζ_{1B}x1.2 and ζ_{1T}x1.3	3.23 (0.61%)	8.86 (0.73%)	4.68(0.42%)	5.20 (3.84%)
2	ζ_{1B}x1.5 and ζ_{1T}x1.5	3.21 (1.23%)	11.07 (0.68%)	4.64(1.27%)	5.88 (5.77%)
3	ζ_{1B}x1.2 and ζ_{1T}x1.8	3.23 (0.61%)	8.79 (-)	4.76(1.28%)	4.51*(47.72%)

The same stepped-sine excitation (frequency range, amplitude and number of cycles), used in the open loop is supplied to the HBMA actuator. The feedback control, generated with the gains designed with the the receptance method ($\mathbf{G}$,$\mathbf{F}$), is added to the stepped-sine signal and the response of the system, filtered, is given to Siemens.PLM LMS Test.Lab to compute the closed-loop input-output FRFs.

By analysing the comparison presented in Table 2 it is possible to notice that the frequencies remain almost unchanged in all the tests considered, instead the damping is increased as expected. The damping of the bending mode is increased as enforced by the control, with an error lower than 1%. Instead, the error on the damping of the torsional mode is higher, and to understand the reasons of this will require further investigations.

Figure 6(a) and 6(b) show a comparison between the fitted FRFs, using SDTools toolbox, for the two laser readings in open loop and close loop. For the close loop it is plotted the case of the test 1, Table 2; the frequencies is kept unchanged, but is possible to observe a small discrepancy in it due to the noise of the original FRFs from which the fitting is built. The damping is decreasing as defined by the controller.

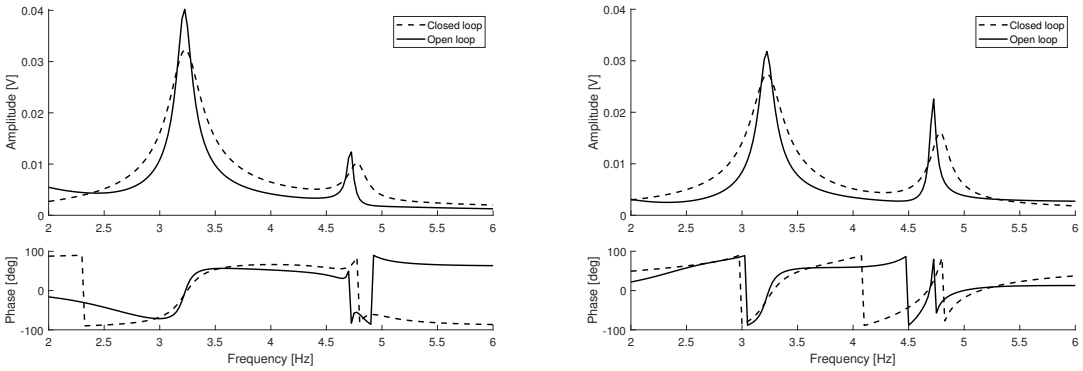

(a) Displacement laser 1.

(b) Displacement laser 2.

Figure 6: FRFs between the two sensor displacement laser and the voltage supplied to the HBMA in open loop and in closed loop.

The velocity vs. frequency and velocity vs. damping diagrams are also computed for the closed loop system. The system is maintained in the same configuration and conditions as for the open loop tests. To compute the diagrams, the controller is tuned as in test 1, Table 2, V-f and V-g

diagrams are plotted in Figure 7(a) and 7(b). As enforced by the controller, both damping are increased, while the frequencies of the bending and torsional modes remain almost the same.

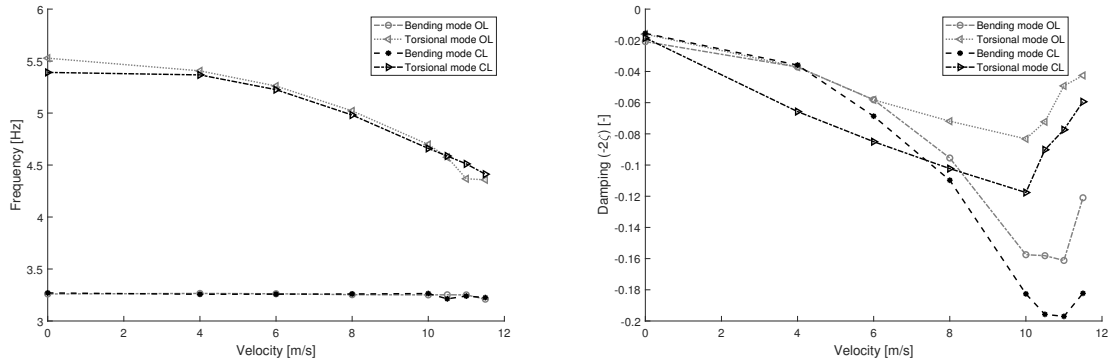

(a) Velocity vs. frequency diagram in closed loop. (b) Velocity vs. damping diagram in closed loop.

Figure 7: V-f and V-g diagrams of the MODFLEX wing in open loop and closed loop.

4.3.1 Flutter control

A flutter test in CL was performed as well, following the same procedure described in Section 4.2. With the controller enabled, the airspeed was increased from 12 m/s until the model became unstable with increments of 0.1 m/s. Table 3 summarises the experiment results, is found that the most efficient way to increase the flutter velocity is by increasing the damping of the torsional mode, this because it is the mode that becomes unstable.

Table 3: Flutter velocity with different control configurations.

	Tests	Flutter velocity [m/s]
	Open Loop	13.30
1	ζ_{1B}x1.2 and ζ_{1T}x1.3	14.10
2	ζ_{1B}x1.5 and ζ_{1T}x1.5	14.30
3	ζ_{1B}x1.2 and ζ_{1T}x1.8	14.40

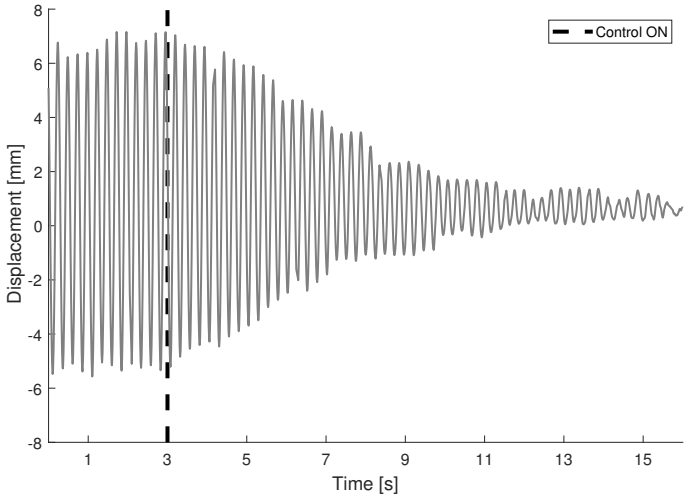

Figure 8: Measured wing displacement at 13.3 m/s (OL flutter velocity) with the control switch on at t = 3 seconds.

Figure 8 shows the effectiveness of the controller while using the test 1 gains, 2. The system is set closed to the OL flutter velocity and while the oscillations of the model are increasing, the HL Controller is switched on (at t = 3 seconds) and the oscillations are quickly damped out.

5 CONCLUSION

The morphing actuator proposed in this work proved to be a suitable alternative to the traditional discrete flap-systems for active control of wind tunnel aeroelastic model. Firstly, the HBMA was tailored for allowing its installation into the MODFLEX aeroelastic rig. Then a receptance-based pole-placement controller was designed for increasing the damping of the first bending and torsional modes and, consequently, attempting to increase the flutter velocity of the system. The actuator proved to be capable to introduce the desired control input and the stability of the overall system was improved. Further development will see the implementation of the PID, not applied in these test configurations, to close the internal loop of the controller and have a better responses of the HBMA. Finally, the controller is set for the system at airspeeds 10 m/s, and it is not adapted for different airspeed, however the control proved to be effective in the cases studied.

6 REFERENCES

[1] Lazarus, K. B., Crawley, E. F., Bohlmann, J. D., et al. (1991). Static aeroelastic control using strain actuated adaptive structures. *Journal of Intelligent Material Systems and Structures*, 2(3), 386–440. ISSN 1045389X.

[2] Wilkie, W., Bryant, R. G., High, J. W., et al. (2000). Low-cost piezocomposite actuator for structural control applications. In *Proceedings of SPIE*, vol. 3991. ISSN 0277786X, pp. 323–334. doi:10.1117/12.388175.

[3] Wilkie, W., G., R., Fox, R., et al. (2003). Positioning monolithic wafers on backing sheets, joining using adhesives, then slicing into fibers and covering with conductive films having electrodes patterns; strain activators. US Patent 6,629,341.

[4] Bilgen, O., Kochersberger, K. B., Inman, D. J., et al. (2010). Novel, Bidirectional, Variable-Camber Airfoil via Macro-Fiber Composite Actuators. *Journal of Aircraft*, 47(1), 303–314. ISSN 0021-8669. doi:10.2514/1.45452.

[5] Molinari, G., Quack, M., Arrieta, A. F., et al. (2015). Design , realization and structural testing of a compliant adaptable wing. doi:10.1088/0964-1726/24/10/105027.

[6] Debiasi, M. and Chan, W.-l. (2016). Measurements of a Symmetric Wing Morphed by Macro Fiber Composite Measurements of a Symmetric Wing Morphed by Macro Fiber Composite Actuators. (January). doi:10.2514/6.2016-1565.

[7] Li, D., Zhao, S., Da Ronch, A., et al. (2018). A review of modelling and analysis of morphing wings. *Progress in Aerospace Sciences*.

[8] Fichera, S., Isnardi, I., and Mottershead, J. E. (2019). High-bandwidth morphing actuator for aeroelastic model control. *Aerospace*, 6(2), 13.

[9] Mokrani, B., Palazzo, F., Mottershead, J. E., et al. (2019). Multiple-input multiple-output experimental aeroelastic control using a receptance-based method. *AIAA Journal*, 1–12.

[10] Ram, Y. M. and Mottershead, J. E. (2013). Multiple-input active vibration control by partial pole placement using the method of receptances. *Mechanical Systems and Signal Processing*, 40(2), 727–735. ISSN 0888-3270. doi:10.1016/j.ymssp.2013.06.008.

[11] Peeters, B., Lowet, G., Van der Auweraer, H., et al. (2004). A new procedure for modal parameter estimation. *Sound and Vibration*, 38(1), 24–29.

COPYRIGHT STATEMENT